# Effects of Poly(3-hexylthiophene) Molecular Weight and the Aging of Spinning Solution on the Electrospun Fiber Properties

Humayun Ahmad, <sup>†</sup> Song Zhang, <sup>‡</sup> Chih-Ting Liu, <sup>‡</sup> Jason D. Azoulay, <sup>‡</sup> Xiaodan Gu, <sup>‡</sup>
Mahesh K Gangishetty, <sup>†</sup> Santanu Kundu<sup>†</sup>\*

<sup>†</sup>Dave C. Swalm School of Chemical Engineering, Mississippi State University, MS State, MS 39762, United States

<sup>‡</sup> School of Polymer Science and Engineering, University of Southern Mississippi, Hattiesburg, MS 39406, USA

Department of Chemistry & Department of Physics and Astronomy, Mississippi State
University, MS State, MS 39762, United States

**Keywords**: Conjugated polymer, P3HT, aging, self-assembly, electrospinning, single fiber, electrical conductivity

#### **ABSTRACT**

The electrospinning technique has been considered an attractive route for processing conjugated polymers in a significant quantity for large-scale applications. The processing-structure-property relationship of the electrospinning process for conjugated polymers is not well understood. Here, we report the electrospinning of poly(3-hexylthiophene) (P3HT) for three different molecular weights of P3HT: 31, 58, and 83 kDa. Chloroform was used as a solvent, and a high molecular weight poly(ethylene oxide) (PEO) was utilized to facilitate the processing of P3HT. The electrospinning was performed on the freshly prepared and 24 h aged spinning solutions. The aging of the spinning solution led to the self-assembly of P3HT chains, particularly with dominant Haggregation for 83 kDa P3HT. The structure development and properties of the fibers were investigated, including the single-fiber electrical conductivity measured using a custom-built setup. The electrical conductivity has been found to be increasing with increasing molecular weight. The self-assembled structure in the aged spinning solution was retained during the electrospinning process, and as high as a five-fold enhancement in single fiber electrical conductivity was obtained compared to the fiber from the freshly-prepared solution. Despite a 25% PEO concentration in the fibers, the maximum electrical conductivity of a single fiber was found to be  $\approx 2.7 \, X \, 10^{-5}$  S/cm, similar to the pristine P3HT thin films. Our study provides a new understanding of structure development as a function of polymer molecular weight and processing steps and relates the structure to the fiber properties.

#### INTRODUCTION

Conjugated polymers (CPs) are being investigated for many applications, including in organic electronics, actuators, sensors, smart apparel, and solar cells, to name a few.<sup>1–9</sup> Several strategies, including developing new polymer architecture and tuning their molecular weight, controlling regioregularity, aging of the processing solution, controlled deposition methods (shear-aligning coating, slow solvent evaporation), and post-deposition treatments (thermal annealing, solvent vapor annealing) have been utilized to achieve the improvement of the charge transport properties in CPs.<sup>6,9–17</sup> However, most of the methods described above mostly involved thin films and were much less investigated in the context of micro- and nanofibers. Although the electrospun fibers can potentially be used in many large volume applications,<sup>4,18–20</sup> a fundamental understanding of the processing-structure-property relationships for the electrospinning process of CPs is still incomplete.

Among different CPs, electrospinning of poly(3-alkylthiophene) (P3AT), especially poly(3-hexylthiophene) (P3HT), has been investigated in the past.<sup>5,20–22</sup> CPs generally have lower molecular weight and are less flexible because of their rigid backbone, and have limited solubility in common organic solvents.<sup>23</sup> As a result, CPs usually do not reach the sufficient chain entanglements in the solution required to form fibers through the electrospinning process. Different strategies have been used to aid the electrospinning process, such as adding flexible polymers, poly(ethylene oxide) (PEO) and poly(£-caprolactone), in the spinning solution of P3HT, or using a core-shell coaxial electrospinning strategy using poly(methyl methacrylate) (PMMA).<sup>5,20,21,24,25</sup> The usage of high molecular weight of PEO is common, which has shown to lead to a uniform, bead-free fibers.<sup>20,22,24–26</sup> Interestingly, few studies have also reported the electrospinning of P3HT without adding any flexible polymers.<sup>23,27–29</sup> Although high P3HT concentration led to gelation,

electrospun fibers were still obtained.<sup>23,28</sup> But, the mechanism for the fiber development from the gel state was not elaborated. For commonly studied flexible polymers, the effects of viscosity and entanglement of polymer solutions on the spinning process have been widely investigated.<sup>30</sup> However, the rheological behavior of P3HT spinning solutions where the self-assembly of polymer chains often leads to gelation has not been well studied.

For thin films, it has been observed that the lower molecular weight of the P3HT lead to a higher crystallinity, at the expense of the tie chains between different crystallites, whereas the higher molecular weight of P3HT leads to disordered structures but better connectivity between the crystallites through long tie chains. 13,31,32 To control the intra- and intermolecular ordering of polymer chains in thin films, preaggregation or self-assembly of P3HTs chains in solution, facilitated by adding a small amount of poor solvent to the polymer solution, ultrasonication, lowering the temperature, and aging of the solution, have been investigated. 6.7,15,33,34 The self-assembled CP nanostructures in solution have been shown to improve the electrical properties of the final processed films. 23,35–37 The impact of molecular weight of CPs and their self-assembly in the spinning solutions on electrospinning have not been investigated. Further, polymer chains in thin films can achieve an equilibrium structure; however, that is unlikely in electrospun fibers due to the rapid evaporation of the solvent and the high stretching force during spinning. Therefore, the properties of thin films and fibers are not directly correlated.

In the literature, the charge-transport behavior of P3HT fibers has been mostly quantified through electrical conductivity measurement of the fiber mats rather than for the single fibers.<sup>20,24</sup> Note that the fiber mat conductivity values represent the bulk conductivity, appropriate for continuous film-like materials, but not for fiber mats, which have void spaces in between.<sup>24</sup> Therefore,

conductivity measurement of the single fibers is essential to determine the processing-structureproperty relationship.

Here, we report the electrospinning of P3HT by systematically varying the molecular weight and also by aging the spinning solutions that enhance the self-assembly of P3HT. We have elucidated the self-assembly process of P3HT in the solution state using spectroscopy experiments, and the gelation behavior was monitored using shear-rheometry experiments. The microstructure of fiber was further analyzed by X-ray scattering techniques. We have also determined the electrical conductivity of individual fibers using a custom-built device and linked the conductivity values to the molecular weight and aging of spinning solutions. Our work demonstrates that the P3HT molecular weight and self-assembly of P3HT chains in the spinning solution retained during the electrospinning process affect the electrical conductivity values of the electrospun fibers. Our results will potentially help rationally develop semiconductive polymeric fibers for smart textiles and wearable device applications.

#### **EXPERIMENTAL SECTION**

#### **Materials**

Three poly(3-hexylthiophene-2,5-diyl) (P3HT) samples were procured from Rieke Metals Inc. (Lincoln, NE) with the weight-average molecular weights of 31 kDa, 58 kDa, and 83 kDa. The polymer characteristics as provided by Rieke Metals are reported in Table S1. Note that all of these polymers had a regioregularity of 95 to 96.2 %. Poly(ethylene oxide) (PEO) (MW ≈ 600-1000 kDa), chloroform (>99.5%), Fomblin Y LVAC 14/6 oil (MW ≈ 2.5 kDa) were obtained from Sigma-Aldrich. All chemicals were used as received.

# **Sample Preparation**

Solutions of P3HT and PEO were prepared separately in individual glass vials. Particularly, 30 mg of P3HT was dissolved in 0.5 mL of chloroform, and 10 mg of PEO was added in 0.5 mL of chloroform in separate vials. Then, the vials were tightly sealed, and the solutions were stirred on a magnetic hot plate at 55 °C for two hours. P3HT and PEO solutions were then mixed at the desired ratios, and the mixture was stirred for another hour at 55 °C. In the final solution, the total concentration of P3HT and PEO was maintained at 4% (wt/v). However, four different combinations of P3HT and PEO ratios were considered, as detailed in the results and discussion section below. Table 1 displays the samples considered here, the designated sample names, and their compositions.

Table 1. Compositions of Spinning Solutions and Processed Samples (Fibers/Beads) in Solid-State

Sample name	Spinning solution composition	Fiber/bead composition	Aging
58 kDa	5 wt/v% P3HT MW 58 kDa	100 wt% P3HT MW 58 kDa	None
31 kDa_0 h	3 wt/v% P3HT MW 31 kDa +	75 wt% P3HT MW 31 kDa +	None
	1 wt/v% PEO MW 1000 kDa	25 wt% PEO MW 1000 kDa	
31 kDa_24 h	3 wt/v% P3HT MW 31 kDa +	75 wt% P3HT MW 31 kDa +	24 h
	1 wt/v% PEO MW 1000 kDa	25 wt% PEO MW 1000 kDa	
58 kDa_0 h	3 wt/v% P3HT MW 58 kDa +	75 wt% P3HT MW 58 kDa +	None
	1 wt/v% PEO MW 1000 kDa	25 wt% PEO MW 1000 kDa	
58 kDa_24 h	3 wt/v% P3HT MW 58 kDa +	75 wt% P3HT MW 58 kDa +	24 h
	1 wt/v% PEO MW 1000 kDa	25 wt% PEO MW 1000 kDa	
83 kDa_0 h	3 wt/v% P3HT MW 83 kDa +	75 wt% P3HT MW 83 kDa +	None

	1 wt/v% PEO MW 1000 kDa	25 wt% PEO MW 1000 kDa	
83 kDa_24 h	3 wt/v% P3HT MW 83 kDa +	75 wt% P3HT MW 83 kDa +	24 h
	1 wt/v% PEO MW 1000 kDa	25 wt% PEO MW 1000 kDa	

# **Electrospinning Process**

The electrospinning was conducted using a custom-built setup shown in Figure 1. In this study, electrospinning was conducted on the spinning solutions that were freshly prepared (designated as w/o aged) and was aged for 24 h (designated as w/24 h aged). After mixing the PEO and P3HT-containing solutions in appropriate proportions, the w/o aged solution was transferred to a syringe (spinning syringe) and was electrospun immediately. For the aging process, the mixed solution was left at room temperature for about 24 h in the spinning syringe. In this case, the needle tip was dipped in chloroform to avoid the drying of chloroform leading to clogging of the tips (Figure S1).

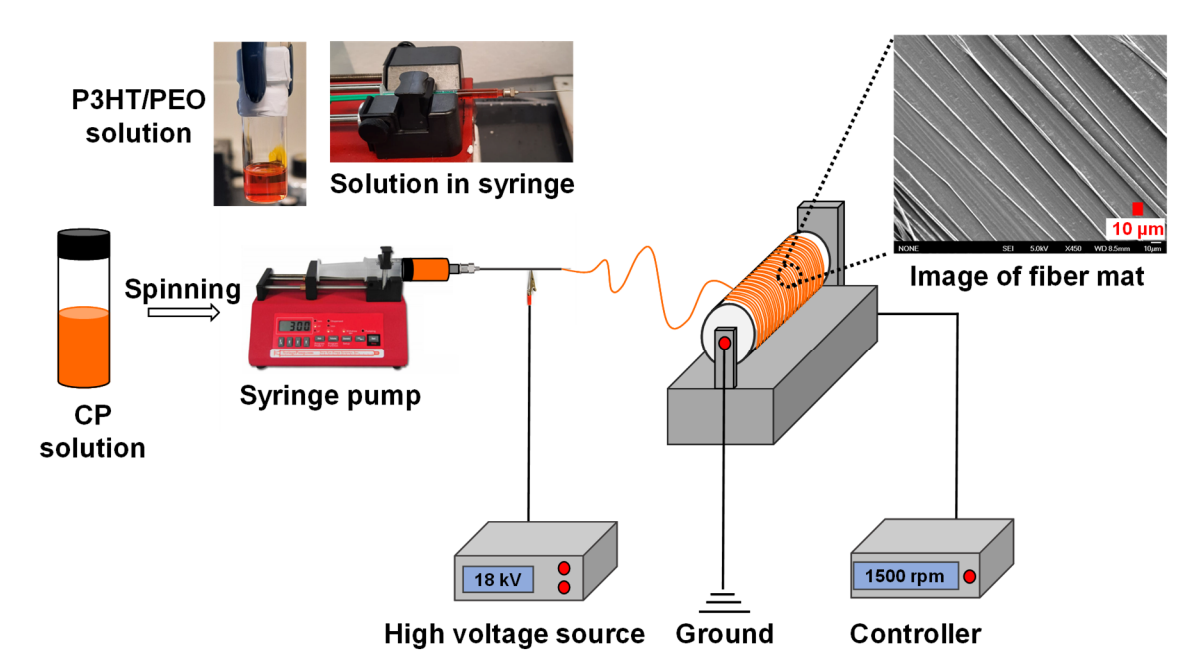


**Figure 1.** Electrospinning setup used for spinning P3HT fibers. Schematic showing spinning steps from solution.

A 1 mL gastight syringe with a 26-gauge flat tip metal needle was used for electrospinning. The syringe with the spinning solution was mounted on a syringe pump (NE-1000, NewEra Pump Systems Inc.). The needle was connected to a high voltage power supply (RC-5000, Tong Li Tech, China) and was placed approximately 8 cm away from a grounded rotating drum collector covered with aluminum foil for sample collections. The rotational speed of the collector was maintained at 1500 rpm for all experiments. The volumetric flow rate was maintained constant at 1.5 mL/h, and 18 kV power was used for all experiments. The needle tip was wiped and cleaned every 30-40 s to prevent the clogging of the needle tip. The experiments were conducted at room temperature (20 °C) with relative humidity ranging from 50 to 60%

# Field-Emission Scanning Electron Microscope (FE-SEM)

A field-emission scanning electron microscope FE-SEM (JEOL JSM-6330F) was used at an accelerating voltage of 5 kV to image the electrospinning fibers. The electrospun fiber mat was collected on aluminum foil and was sputter-coated with an approximately 15 nm thick platinum layer to avoid charging and to enhance the quality of the micrographs. An image processing software (ImageJ) was used to measure the fiber diameters.

# **Rheological Study**

The rheological investigations were conducted using a TA Instruments HR-2 Discovery rheometer equipped with a Peltier stage. A 25 mm parallel plate geometry was used. The samples were loaded on the bottom plate at 20 °C, and a gap of 400 µm between the upper and bottom plates was maintained. In our experimental setup, a petri dish was attached to the bottom plate, and the petri dish was filled with fluorinated oil (Fomblin Y LVAC 14/6) after the sample loading in the parallel plate geometry. The oil level was maintained slightly above the edge of the top plate. This setup (Figure S2) suppressed the chloroform evaporation during the rheological experiments.<sup>38</sup>

# **Photoluminescence Analysis**

The fluorescence study of the P3HT/PEO solution was conducted using an Edinburgh FS5 Spectrofluorometer instrument. A 4 mL quartz cuvette of 1-cm path length was used to investigate solutions, whereas thin film and fiber mats were collected on 15 mm by 20 mm quartz coated glass substrates. The excitation wavelength of 450 nm was used, and the emission scans were recorded over the range of 465 to 800 nm using a slit width of 2-5 nm with a 1 nm wavelength increment and an integration time of 1 s.

# **Thermal Analysis**

The thermal properties of electrospun fibers were analyzed using a TA instrument DSC-Q2000. DSC measurements were performed under a nitrogen atmosphere at the heating rate of 5 °C min<sup>-1</sup> from -50 °C to 330 °C. Hermetically sealed aluminum pans with a sample weight varying from 2 to 5 mg were used.

# X-ray Diffraction (XRD) and Grazing Incident Wide-Angle X-ray Scattering (GIWAXS)

XRD patterns were recorded in a Rigaku Ultima IV X-ray diffractometer (CuK $\alpha$ -radiation;  $\lambda$ =0.154 nm) with a scanning rate of 0.5°/min over the 2 $\theta$  range of 3° to 30°. P3HT thin film and fiber mats for XRD measurements were deposited on a quartz-coated glass slide. Furthermore, the P3HT chain orientation in fiber was investigated using grazing incident wide-angle X-ray scattering (GIWAXS). A thin layer of electrospun fiber mat was collected on the Si wafer by placing it on the collector. GIWAXS measurements were conducted on XENOC Xeuss 2.0. An incident X-ray energy of 8.05 keV at an incident angle of 0.2° was used. The data was collected using the Pilatus 1M detector and analyzed in Igor 8 software using Nika package and WAXStools.

# **Electrical Conductivity**

A custom-built multipin framework was used to measure the electrical conductivity of single electrospun fibers (Figure S3). Here, a quartz-coated glass substrate with an array of gold contacts was fabricated (chips). The gold contacts were deposited via thermal evaporation. The distance between two adjacent gold contacts varied between 30 to 80 µm. Electrospun fibers were collected on these chips. For this, electrospinning was performed for a short time, and a limited number of fibers (1-4) connecting two neighboring contacts was identified by an optical microscope image. A custom-built multipin system was used to measure the I-V responses over -2 V to 2 V using a Keithley source meter (2604B, dual-channel, 40V SMU). A minimum of three batches obtained from different spinning solutions and at least four samples from each batch, i.e., on an average 12 samples were considered for each condition.

In addition, fiber mat conductivity was measured using an electrode system (IDE) from Metrohm Dropsens (Spain). The IDE has two planar interdigitated electrodes (bands/gaps: 10  $\mu$ m, number of digits: 125 × 2) with two connection tracks made of platinum, fabricated on a glass substrate (L 22.8 × W 7.6 × H 0.7 mm). A thin layer of fiber mat covering the IDE's active area was collected by placing the IDE chips on the rotator. A potential was applied between the two probes using Keithley 2450 source meter. The conductivity ( $\sigma$ ) of the fiber mat was calculated from the measured resistance (R) of the fiber mat and the cell constant of the IDE (K) using the relationship of  $\sigma = \frac{K}{R}$ , where K is the cell constant of the IDE chip.

# RESULTS AND DISCUSSION

# **Electrospinning and Morphology of Electrospun Fibers**

Three different molecular weights (MWs) of P3HT, 31, 58, and 83 kDa were considered here. For each molecular weight of P3HT, the spinning was performed using the freshly prepared and 24 h

aged solutions. This allowed us to investigate the effects of aging on the self-assembly of P3HT in the spinning solution and the corresponding impacts on the fiber properties. The freshly prepared solution (w/o aged) at 55 °C was rapidly transferred to the syringe. The temperature dropped to room temperature at ~10 mins (Figure S4), and the spinning was conducted at room temperature. Both the aging of the spinning solution (w/24 h aged) and the subsequent spinning was conducted at room temperature without further heating of the solution.

The electrospinning of P3HT in chloroform was initially attempted considering three different P3HT (Mw: 53 kDa) concentrations: 5, 8, and 12 wt/v%. The 5 and 8 wt/v% solutions resulted in bead formation (Figure 2a-b), whereas 12 wt/v% solution was too viscous to process, resulting in only a few beads on aluminum foil (Figure S5). Similar results have been observed for the other two molecular weights of P3HT considered here. We hypothesize that the P3HT chains rapidly formed a gel-like structure at room temperature. Although such structure likely dissociated as it flowed through the needle, there were no significant entanglements of polymer chains necessary for fiber formation for the concentration and molecular weights considered here. <sup>24,39,40</sup> Note that P3HT backbone rigidity results in a high entanglement molecular weight. <sup>24</sup>

A high molecular weight PEO (MW~600-1000 kDa) was added to the P3HT solutions to circumvent this problem. PEO of this molecular weight has a significant chain entanglement, and it was possible to spin fibers from 1 to 4 wt/v% solutions of only PEO in chloroform (Figure S6). The PEO concentration and the P3HT to PEO ratio were varied to determine the suitable processing window while maintaining the total polymer (P3HT + PEO) concentration of 4 wt/v%. Four different concentrations of P3HT ( $M_w \approx 83$  kDa), 4%, 3.9%, 3.6%, and 3% were considered. As discussed above, 4 wt% (no PEO added) did not lead to fiber formation, whereas 3.9 and 3.6 wt% resulted in beaded fibers (Figure 2c, S7). For 3 wt/v%, smooth fibers were obtained.

Therefore, the beads progressively disappeared with increasing PEO concentration in the spinning solution (Figure S7), and such observations were true even for the 24 h aged spinning solution (Figure 2d), and for all MWs of P3HT considered here (Figure 2h-j). We have considered 3 wt/v% P3HT with 1 wt/v% PEO for further detailed investigations (Table 1). For each case, we could conduct electrospinning for 30 minutes, indicating the stability of our process/system.

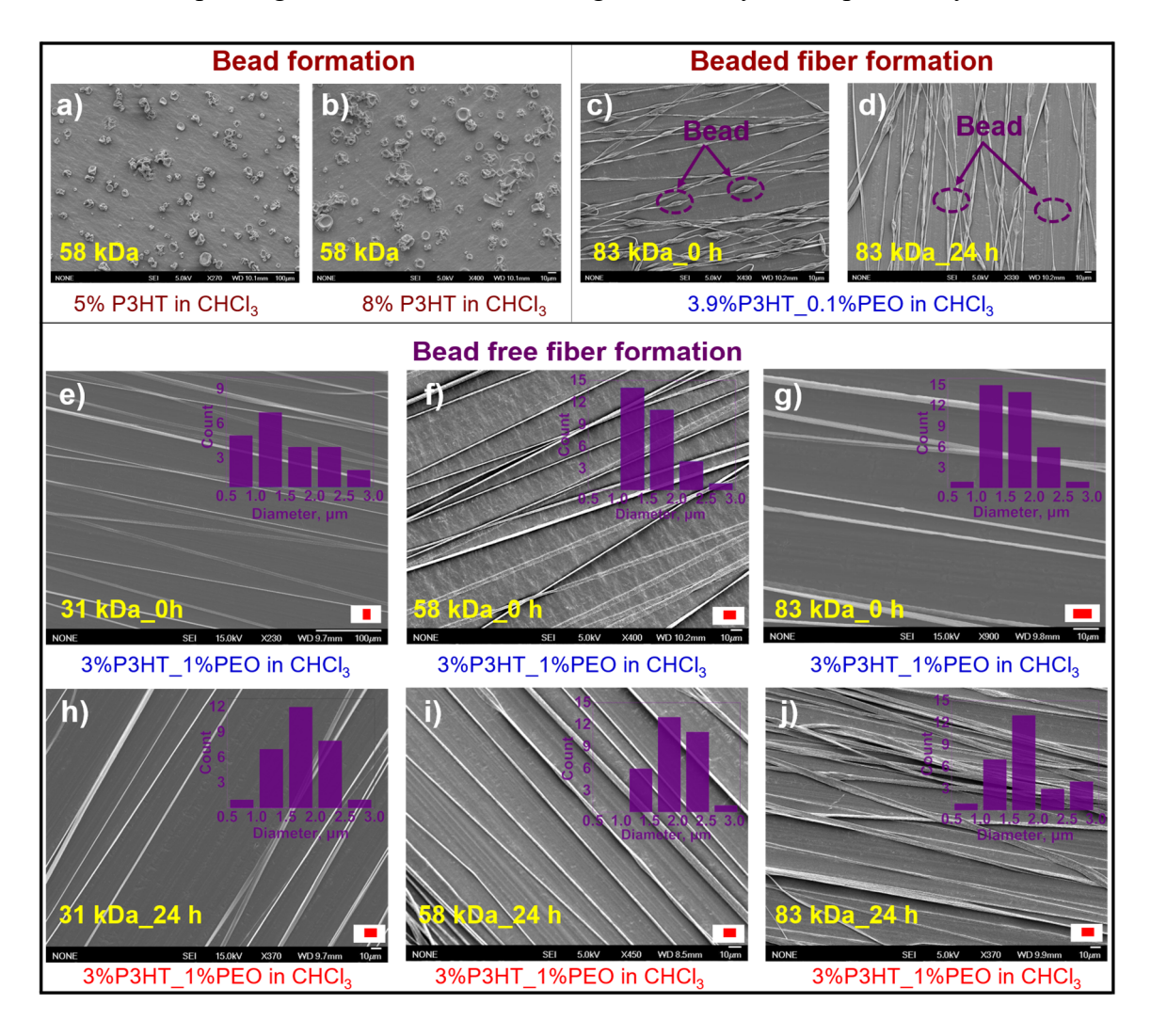


**Figure 2.** SEM micrographs of samples collected on aluminum foil. (a,b) Bead formation of P3HT without PEO; (c,d) Beaded fibers obtained from 3.9% P3HT (83 kDa) solution. Bead free fibers obtained from 3% P3HT solutions of different molecular P3HT weights with and without aging: (e,h) 31 kDa, (f,i) 58 kDa, and (g,j) 83 kDa. Scale bars represent 10 μm.

As observed in SEM images, the fibers were mostly cylindrical (Figure S8). The fiber diameters were measured from the SEM images, and the corresponding histograms for at least 30 individual fibers for each case are shown as insets in Figure 2e-j. These histograms indicate mostly one dominant fiber diameter. For the fibers obtained from w/o aged spinning solutions, the average fiber diameters (Figure 2e-g) were 1.80, 1.68, and 1.67 µm for 31 kDa, 58 kDa, and 83 kDa MWs of P3HT, respectively. For w/24 h aged spinning solutions, the average fiber diameters (Figure 2h-j) were 1.70, 1.98, and 2.0 µm for 31 kDa, 58 kDa, and 83 kDa MWs of P3HT, respectively. Without aging, the fiber diameters for 58 and 83 kDa samples were similar, but 31 kDa fibers had a slightly larger diameter. With aging, a small increase in fiber diameter was observed for 58 kDa and 83 kDa, however, the t-test indicates that the difference was not statistically significant. Note that the fiber diameters reported here are larger than the typical sub-micron length scale typically reported for electrospun fibers.<sup>20,21</sup> We have also been able to obtain fibers with such lower diameters (Figure S9), but not considered here, as electrical conductivity measurement (as reported below) for such smaller diameter fibers was extremely challenging.

# **Interpreting Self-Assembly of P3HT in the Spinning Solution**

The freshly prepared solutions consisting of P3HT, and PEO had bright orange color, indicating their fully dissolved state. However, the solution color with 83 kDa P3HT changed from bright orange to an opaque, dark red/ purple with time as it was aged in a syringe needle for 24 h (Figure S10). After 24 h of aging, the solution became gel-like. The color change and gelation indicate the self-assembly of the P3HT chains. For 31 kDa P3HT, the solution only became slightly viscous, and the color change was insignificant, as it remained bright orange after 24 h of aging (Figure S11). The self-assembly of polymer chains in the solutions was determined by investigating their photophysical properties.

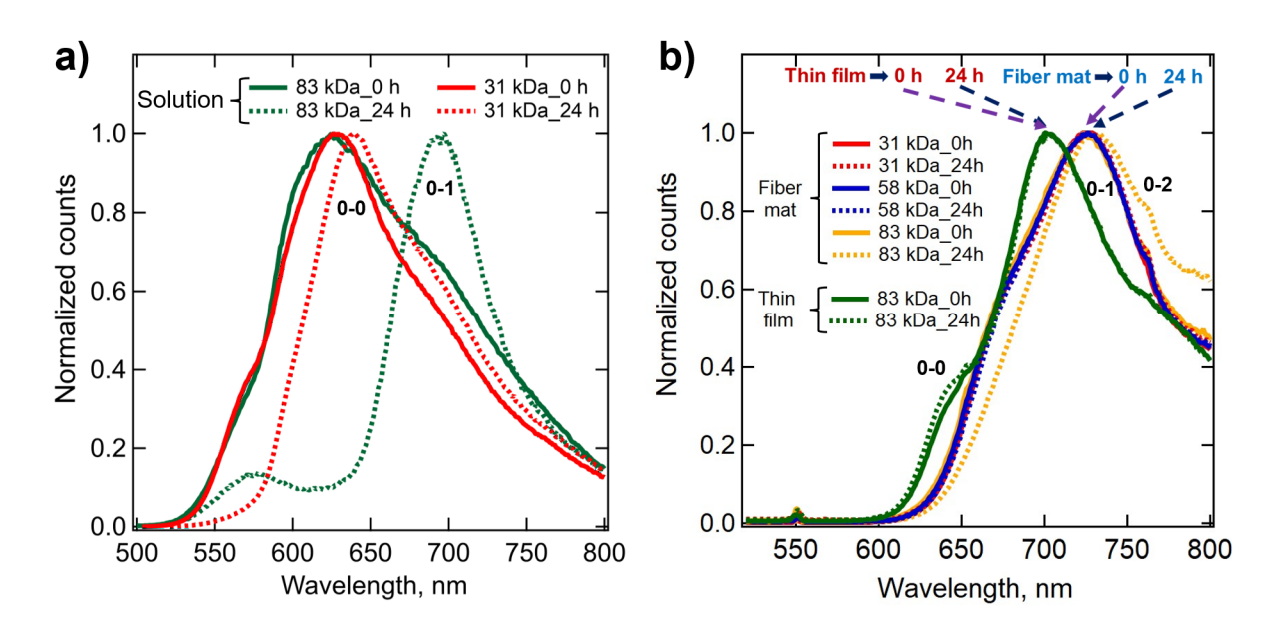


**Figure 3.** Photoluminescence spectra of (a) solutions with 83 kDa P3HT w/o and w/24 aging; b) thin film and fiber mats with different P3HT molecular weights obtained from solutions w/o and w/24 aging. The excitation wavelength was 450 nm.

Figure 3a displays photoluminescence (PL) spectra of w/o and w/24 h aged solutions with 31 kDa and 83 kDa excited at 450 nm. For w/o aged solutions, one broad peak at  $\approx$ 633 nm and two shoulders around 550 nm and 680 nm were observed. A clear peak around 641 nm and a shoulder around 700 nm were observed for w/24 h aged solution of 31 kDa. In contrast, one broad peak around 580 nm and a relatively sharp peak at 697 nm were observed for 83 kDa w/24 h aged solution. The peaks at 550 and 580 nm have been attributed to the amorphous state of P3HT, associated with the  $\pi$ - $\pi$ \* transition.<sup>43</sup> The development of the 697 nm peak for 83 kDa can be attributed to the aggregation of P3HT chains,<sup>43</sup> confirms the self-assembly of P3HT chains during aging, even in the presence of PEO. It has been shown earlier that self-assembly and gelation of P3HT in solution in the presence of another component are possible, for example, for P3HT and di-Fmoc-l-lysine (a low molecular weight gelator) system in chloroform, provided P3HT and the

other component are not interacting.<sup>25,26,38</sup> However, for 31 kDa w/24 h aged solution, the PL data was not significantly different from the w/o aged one, and only an 8-10 nm redshift of the 633 nm aggregation peak was observed. Therefore, no significant self-assembly took place in that sample.

Next, we investigate how the self-assembly in the solution state transformed into the solid-state (fibers and films). The w/o and w/24 h aged solutions of 83 kDa P3HT were deposited as thin films on quartz plates, and the PL data of those thin films are shown in Figure 3b. For thin-film, no significant changes in peak positions occurred due to the solutions' aging. A similar trend was also observed for the other two MWs of P3HT (Figure S12)

The PL data for the fiber mats collected on the quartz slides are also shown in Figure 3b. The results for all fibers except for the fibers obtained from 24 h aged solution of 83 kDa of P3HT (83 kDa\_24h) were very similar. Specifically, for all samples, except for 83 kDa\_24h, a broad shoulder at 660 nm and a prominent peak at 724 nm were observed. For the 83 kDa\_24h P3HT, a peak at ≈732 nm was observed, but there was no shoulder peak.

The peaks at  $\approx$ 633 nm in solutions,  $\approx$ 630 nm in thin films, and  $\approx$ 660 nm in fibers correspond to the 0-0 vibronic transition of P3HT. Whereas the peaks at  $\approx$ 698, 703, and 724 nm for the solutions, thin films, and the fiber mat, respectively, represent the 0-1 vibronic transition of P3HT. Further, 0-0 and 0-1 transitions are related to the J- and H- aggregates, representing the intrachain and interchain exciton coupling, respectively. The dominant aggregation type can be hypothesized based on the intensity ratio,  $I_{0-0}/I_{0-1}$ . For the 31 kDa\_0h, 31 kDa\_24h, and 83 kDa\_0h solutions,  $I_{0-0}/I_{0-1}>1$  was observed, indicating significant intrachain coupling (J-aggregate) instead of interchain one. In comparison, 83 kDa\_24h solution displayed  $I_{0-0}/I_{0-1}<1$ , signifying a predominantly H-aggregated system. The change from J- to H-aggregates in 83 kDa\_24h aged

solution indicates that the self-assembly during solution aging increased the interchain exciton coupling by promoting  $\pi$ - $\pi$  stacking of P3HT chains.<sup>43,44</sup> This is also relevant to the significant solution color change due to the aging discussed above.

For both thin-film and fibers,  $I_{0-0}/I_{0-1} < 1$  signifies that the H-aggregation dominated over the J-aggregation. Interestingly, the PL data did not capture any detectable peak for the 0-0 band in 83 kDa\_24h fibers. Thus, the H-aggregates fraction was much higher in 83 kDa\_24h fibers than the fibers from both w/o and w/24h aged 31 kDa solutions. Further, in comparison to the thin film, the aggregation peaks for the fibers red-shifted as high as 31 nm (83 kDa\_24h), higher than that typically reported in the literature.  $^{26.48}$  The high molecular weight (83 kDa) and regioregularity (95%) of the P3HT sample used in this study have facilitated the self-assembly process during aging, and the self-assembled structures retained in the electrospun fibers. Further, the electric field applied during the electrospinning process caused the extension of PEO and P3HT chains along the applied electric field direction. This likely promoted further  $\pi$ – $\pi$  stacking of existing non-aggregated P3HT chains, resulting in an increase of H-aggregates. Note that we have observed a maximum  $\pm 4$  nm peak shift between experiments because of small fluctuations of P3HT and PEO weight ratios and slight variation in the sample preparation conditions (hot plate temperature, relative humidity), however, the overall trend remained the same.

# **Rheological Response of Spinning Solutions**

As the self-assembly of P3HT in the solution can lead to changes in rheological responses affecting the spinning behavior, we conducted shear-rheometry at room temperature on the w/o and w/24h aged solutions of 31 kDa and 83 kDa P3HT using the custom-built setup shown in Figure S2.

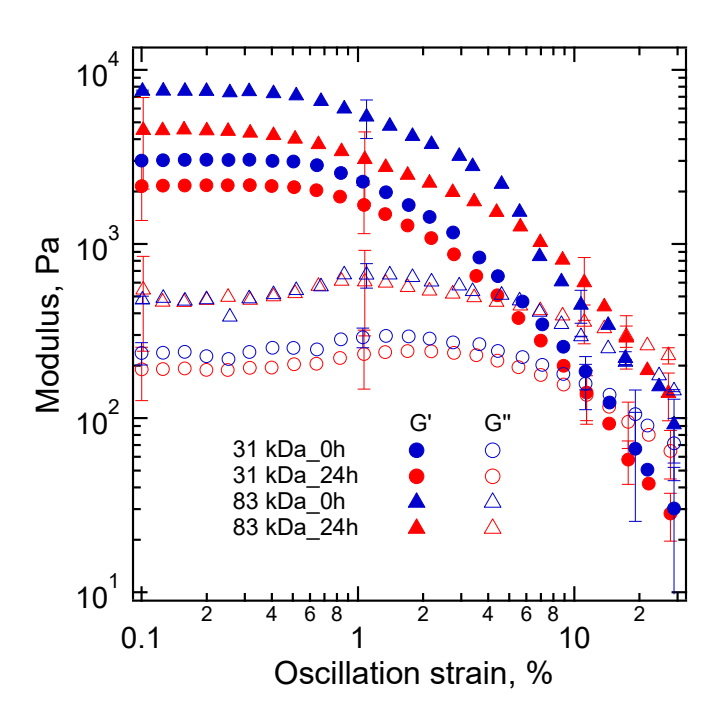


**Figure 4.** Storage (G') and loss (G") moduli as a function of oscillation strain amplitude captured at the frequency ( $\omega$ ) of 1 rad/s and room temperature of 20 °C. Representative error bars are shown.

Figure 4 displays the storage (G') and loss (G") moduli as a function of oscillation strain amplitude  $(\gamma_0)$  for the solutions of 31 kDa and 83 kDa P3HT. For  $\gamma_0 < 0.5\%$ , G' was higher than G" and was independent of  $\gamma_0$ , indicating soft-solid or gel-like behavior. However, for  $\gamma_0 > 0.5\%$ , G' decreased with applied strain. In addition, G" slightly increased for  $\gamma_0 > 0.6\%$  and then decreased for  $\gamma_0 > 1\%$ . A crossover of G' and G" was observed at a higher  $\gamma_0$  value. These results signify that the underlying structure was disrupted at higher strain amplitude, and the sample became more fluid-like. For both molecular weights, a decrease of G' and G" was observed with aging; particularly, a significant drop in G' for 83 kDa\_24h P3HT has been observed. At this stage, the origin of such a decrease with aging is unknown and will be further investigated in a future study.

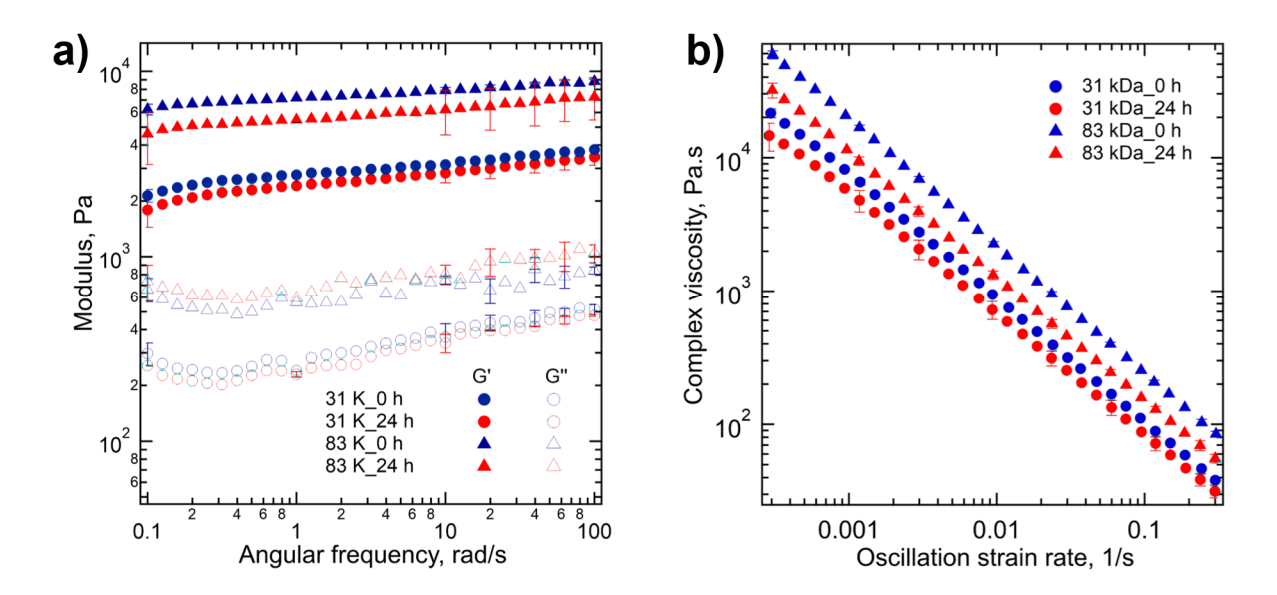


**Figure 5.** a) G' and G" as a function of frequency, and b) complex viscosity vs. oscillation strain rate. Representative error bars are shown.

Figure 5a displays G' and G" as a function of angular frequency for the samples w/o and w/24 h of aging. Frequency sweep experiments were performed over the frequency range of 0.1–100 rad/s using an oscillation strain amplitude of 0.3%, which was within the LVE region. Both G' and G" displayed weak frequency dependency, further capturing the soft solid-like behavior of these samplers at low strain amplitude, as observed in the amplitude sweep experiments.

The gelation of the P3HT and PEO in chloroform has not been reported in the literature. However, the gelation behavior of pure P3HT solution at high concentrations and a system consisting of low concentrations of P3HT and a low molecular weight gelator have been reported earlier. <sup>38,53–56</sup> In those gels, the P3HT chains have been shown to self-assemble to form nanofibers. Besides, those gel systems have moduli similar to that presented here. <sup>54–56</sup>

The estimated complex viscosity values as a function of the oscillation strain rate are shown in Figure 5b. It was difficult to obtain shear-viscosity data at high shear rates for our samples (steady shear viscosity over a limited shear rate range is presented in Figure S13); therefore, we are

considering complex viscosity as a function of oscillation strain rate as the representative shearrate dependent response. Although the applicability of the Cox-Mertz rule for this system was not verified here, the complex viscosity values can provide some additional insights. The complex viscosity decreased with increasing oscillation strain rate for both samples.

The shear and extensional viscosity values have been shown to affect the spinnability of a polymer solution, <sup>57</sup> however, the spinnability of a gel-like system is not well understood. We estimated the wall shear rate for the volumetric flow rate (Q) considered here as  $\dot{\gamma}_w = \frac{4Q}{\pi R_N^3} \sim 250 \text{ s}^{-1}$ . Here,  $R_N$  the internal radius of the needle. By considering the shear-thinning behavior observed in Figure 5b, the viscosity values at these shear/strain rates were low, and it was possible to electrospun the solutions. We hypothesize that the weak gel-like sample dissociated into a viscous solution because of the shear stress as it flowed through the needle. Note that the shear viscosity did not decrease monotonically with  $\dot{\gamma}$  and the response was slightly different from the complex viscosity, but the underlying mechanism was not investigated as it was beyond the scope of this manuscript.

#### **Thermal Behavior of Fiber Mats**

Both P3HT and PEO are semicrystalline polymers, and it is expected that these polymers form crystalline domains within the fibers. We used a differential scanning calorimeter (DSC) and x-ray diffraction (XRD) to investigate these. The measured melting temperatures of bulk P3HT used here were ≈240.8 (31 kDa), 244.8 (58 kDa), 247.1 °C (83 kDa), and that for PEO powder and PEO fibers were 67.5, and 59.5 °C, respectively (see Figure S14 and Figure S15 for the thermograms), values similar to that reported in the literature. <sup>21,58</sup>

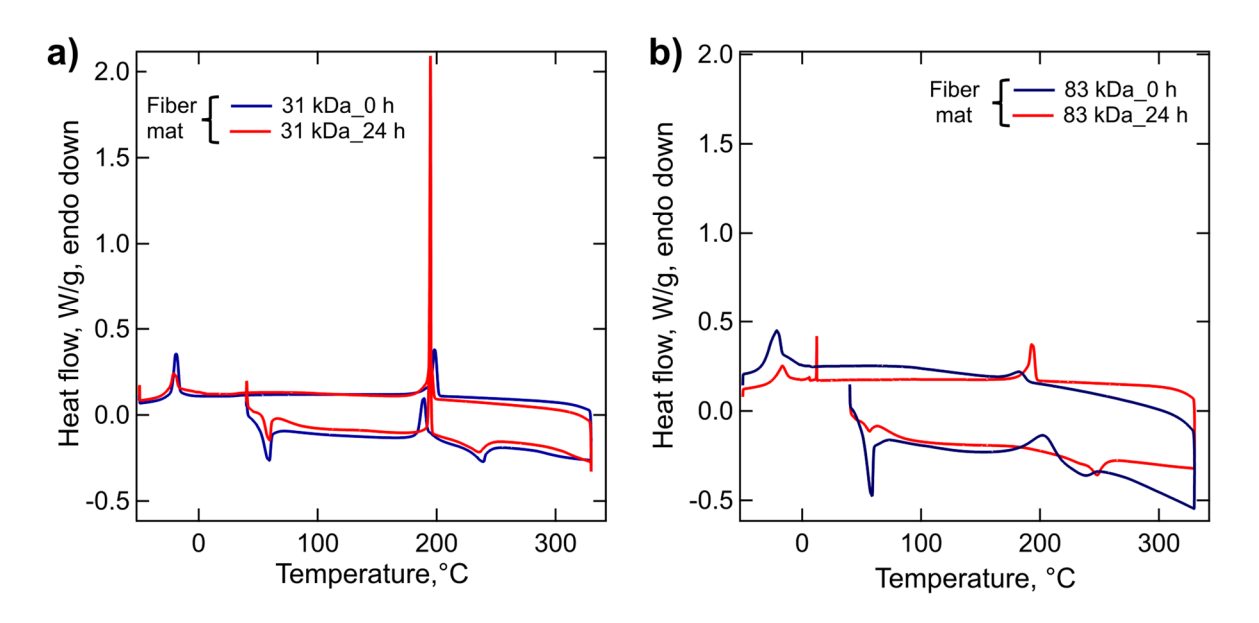


**Figure 6.** Differential scanning calorimetry results (first heating and cooling scan) for the electrospun fibers: a) 31 kDa P3HT, b) 83 kDa P3HT.

Figure 6a displays DSC thermograms for 31 kDa\_0h and 31 kDa\_24h fibers. For 31 kDa\_0h fibers, two endothermic peaks at  $\sim$ 59.5 and 238 °C in the first heating cycle capture the melting of PEO and P3HT, respectively. For the 31 kDa\_24h fibers, PEO and P3HT melting temperature did not change significantly in comparison to 31 kDa\_0h fibers. These were also in the same range as obtained for pristine P3HT and PEO samples. In addition, a sharp exothermic peak at 195 °C was observed for the 31 kDa\_24 h fibers, however, the peak was less sharp (at  $\approx$  190 °C) for the 31 kDa\_0 h fibers. This exothermic peak was likely due to the recrystallization of P3HT. For PEO fibers without P3HT such a peak was not observed. As expected, in the second heating cycle, the recrystallization peak was not observed (Figure S16). The exothermic peaks in the cooling cycle captured the crystallization of P3HT and PEO components.

For 83 kDa\_0h fibers (Figure 6b), similar to the 31 kDa fibers, melting peaks at ~60 °C (PEO) and ~240 °C (P3HT) were observed. In 83 kDa\_24h fibers, the PEO melting peaks remained similar, but the P3HT melting peak shifted from 240.2 °C to 248.5 °C, indicating the presence of a more

ordered (crystalline) structure in that sample.<sup>21</sup> For 83 kDa\_0h fibers, a recrystallization peak at 205.5 °C was observed, however, such a clear peak was not observed for 83 kDa\_24h fibers.

The recrystallization peaks indicate that the highly volatile chloroform rapidly evaporated from the electrospun fibers, suppressing the crystallization of P3HT. Those kinetically frozen chains started to recrystallize in the first heating cycle. For the 83 kDa\_24 h fibers, the chains were already highly self-assembled, and during heating in DSC experiments, further crystallization did not take place. The overall crystallinity measurement for this sample also supports this behavior. The degree of crystallinity for 83 kDa\_24 h fibers was estimated as  $\approx 71.5\%$ , considering the enthalpy of fusion  $\Delta H_u \approx 49 J/g$  as reported by Snyder et al., whereas that for the as-received pristine 83 kDa P3HT powder was  $\approx 51\%$ . The crystallinity of 83 kDa\_24h fibers was higher than the reported typical crystallinity values of P3HT samples. Note that we were not able to estimate the crystallinity for other fibers with the recrystallization peak.

#### Microstructure of the Fibers

The microstructure of the pristine P3HT, PEO powders, drop-casted pure P3HT and P3HT/PEO thin films, fiber mats for different molecular weights of P3HT, and aging conditions have been investigated using XRD. Figure 7a displays the normalized XRD spectra (data without normalization are shown in Figure S17) collected for pristine P3HT thin film (58 kDa), P3HT/PEO thin films (P3HT 83 kDa) from w/o and w/24 h aged solutions. For thin films, the solutions were drop-casted on a quartz-coated glass substrate and were slowly dried to facilitate the self-assembly of P3HT chains.

The pristine P3HT thin-film displayed characteristic peaks at  $2\theta \approx 5.3^{\circ}$ ,  $10.8^{\circ}$ , and  $16.3^{\circ}$  related to the (100), (200), and (300) planes, respectively. For pristine PEO thin film, the peaks at  $2\theta \approx 19.1^{\circ}$  and  $23.3^{\circ}$  (Figure S18) are for the (120) and (112) planes, respectively. <sup>59</sup> The P3HT/PEO thin film

from w/o and w/24 h aged solutions displayed the presence of all characteristic peaks of P3HT and PEO. However, the peak at ~23° was sharper for the 83 kDa\_24 h. This could be an overlap of the (010) peak of P3HT and (112) peak of PEO. The (010) peak corresponds to the interchain  $\pi$ - $\pi$  stacking of P3HT.<sup>21,62</sup> The strong (100) P3HT peak indicates lamellar stacking in P3HT, both with and without PEO.<sup>20,21</sup> Note that different peak intensity was considered for normalization in each case, as the different peaks displayed the highest intensity for 83 kDa\_0h and 83 kDa\_24h fibers. Specifically, for 83 kDa\_0h fibers, the scattering profile was normalized based on the (120) peak intensity. In contrast, for thin-film and 83 kDa\_24h fibers, the (100) peak intensity was chosen for the normalization.

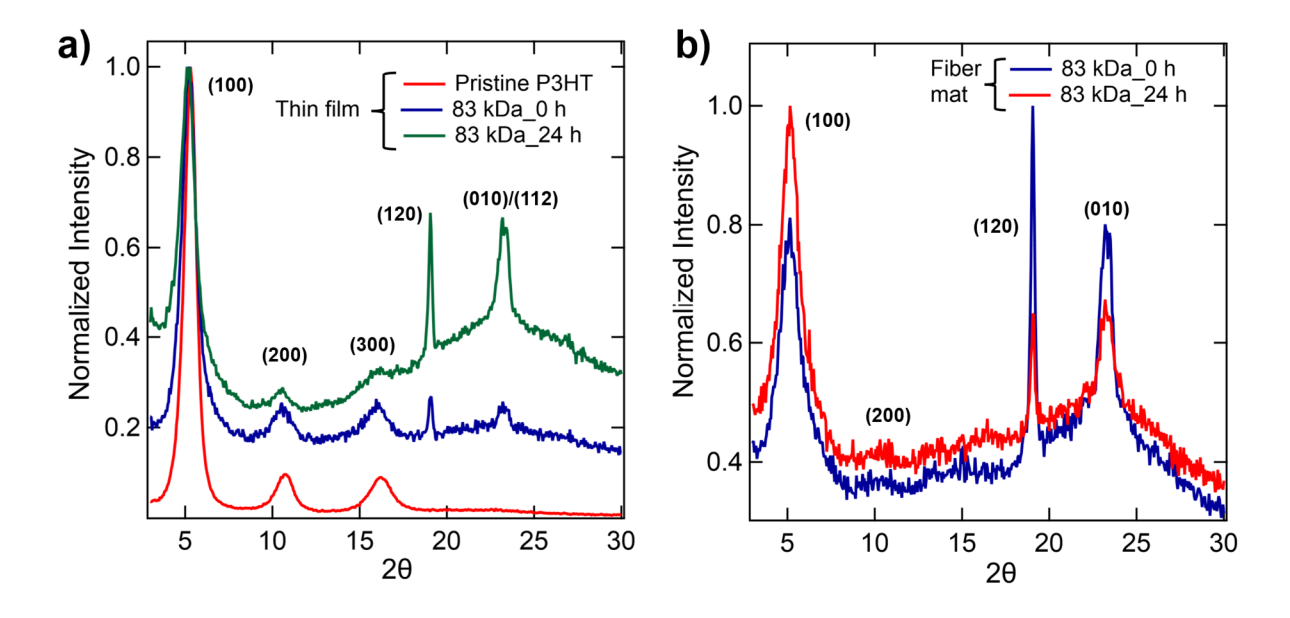


**Figure 7.** X-ray diffraction patterns for: a) thin films of pristine P3HT (58 kDa) and P3HT (83 kDa)/PEO; b) electrospun P3HT (83 kDa)/PEO fiber mats. The (100) peak intensity was considered for the normalization of thin-film data and 83 kDa\_24h fibers, whereas (120) peak intensity was considered for 83 kDa\_0h fibers.

For the fibers (Figure 7b), peaks at  $2\theta = 5.2^{\circ}$ ,  $19.1^{\circ}$ , and  $23.2^{\circ}$  represent the diffraction peaks from (100) planes of P3HT, (120) planes of PEO, and (010) planes of P3HT, respectively. The  $23.2^{\circ}$ 

peak was more pronounced than that observed for the thin film. Thus, both lamellar and  $\pi$ - $\pi$  stacking of P3HT chains were present in the fibers. Note that for pristine PEO fibers, only (120) peak was observed (Figure S18). The absence of (112) peak has been attributed to the small fiber diameter that most likely restricted the size of (112) planes, resulting in a reduction of peak intensity or elimination of the peak.<sup>58,63</sup>

The full-width half maxima (FWHM) values for different peaks have been estimated (Table S2). For the 83 kDa\_24h fibers, the FWHM values for both lamella and  $\pi$ - $\pi$  stacking directions were lower than those observed in the 83 kDa\_0h fibers. The reductions of FWHM further indicate that 83 kDa\_24h P3HT fibers were more crystalline, consistent with the DSC results.

Any possible orientation of crystalline domains in the fibers was investigated by capturing GIWAXS data on the fiber mats. We considered two cases where the incident beam was orthogonal and parallel to the long-axis direction of fibers, as shown schematically in Figure 8a-b. The out-of-plane and in-plane 1D intensity vs. scattering vector plots are shown in Figure 8c-d. The peak anisotropy was obtained by integrating the intensity over azimuthal angle for two peaks over the q ranges of 1.34 to 1.44 Å<sup>-1</sup>, and 1.6 to 1.8 Å<sup>-1</sup>, respectively.

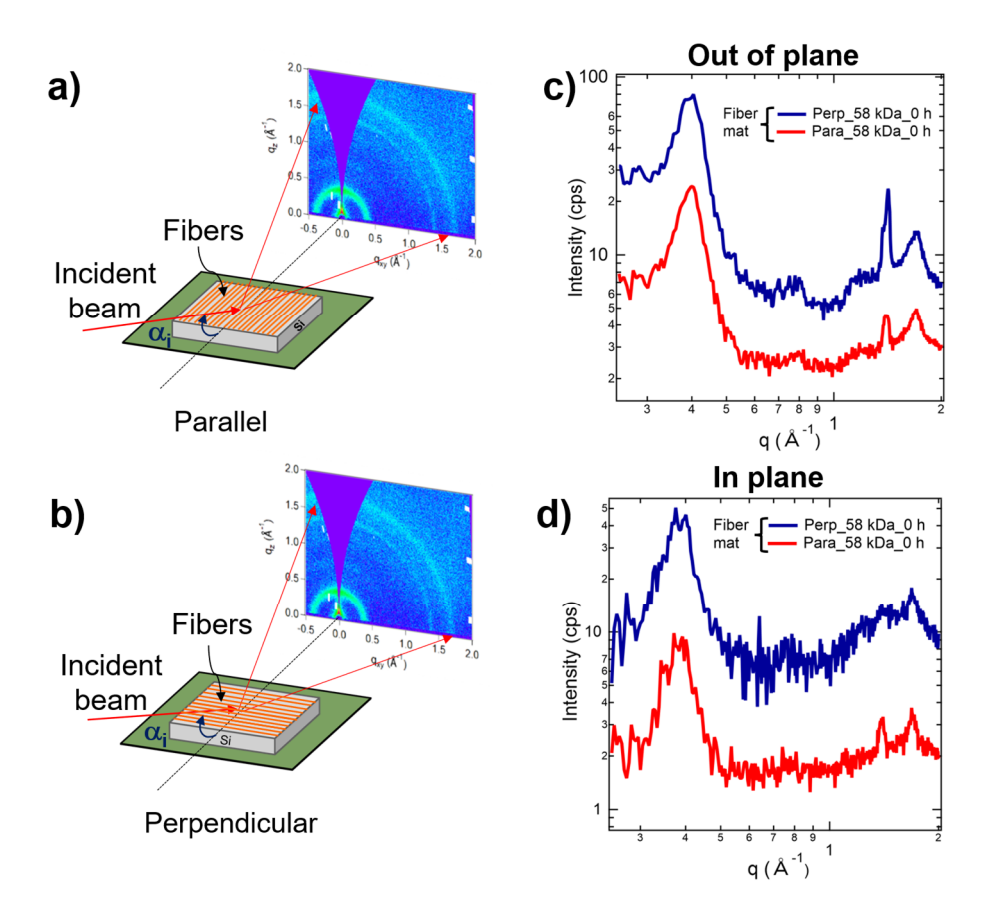


**Figure 8.** 2D GIWAXS patterns of fiber mat for 58 kDa\_0h aligned a) parallel, b) perpendicular to the incident beam direction. 1D GIWAXS profiles for (c) out-of-plane and (d) in-plane directions.

Here, the results for 58 kDa\_0h fibers obtained from w/o aged solution are shown. For the beam direction orthogonal and parallel to the fiber axis, the intensity of the (100) peak was stronger in both q<sub>z</sub> direction (out-of-plane) and q<sub>xy</sub> direction (in-plane). In contrast, the (010) peak was more prominent for out-of-plane than the in-plane direction. These indicate that for this sample, the P3HT chain did not adopt a specific arrangement (edge-on or face-on) with respect to the fiber axis/surface. Instead, P3HT crystals were more randomly oriented in fibers. The fast evaporation rate of solvent inhibited P3HT chains from forming preferential orientation. <sup>21,64,65</sup> The proposed

microstructure for a typical fiber is shown in Figure 9, and this structure can lead to the scattering patterns shown in Figure 8.

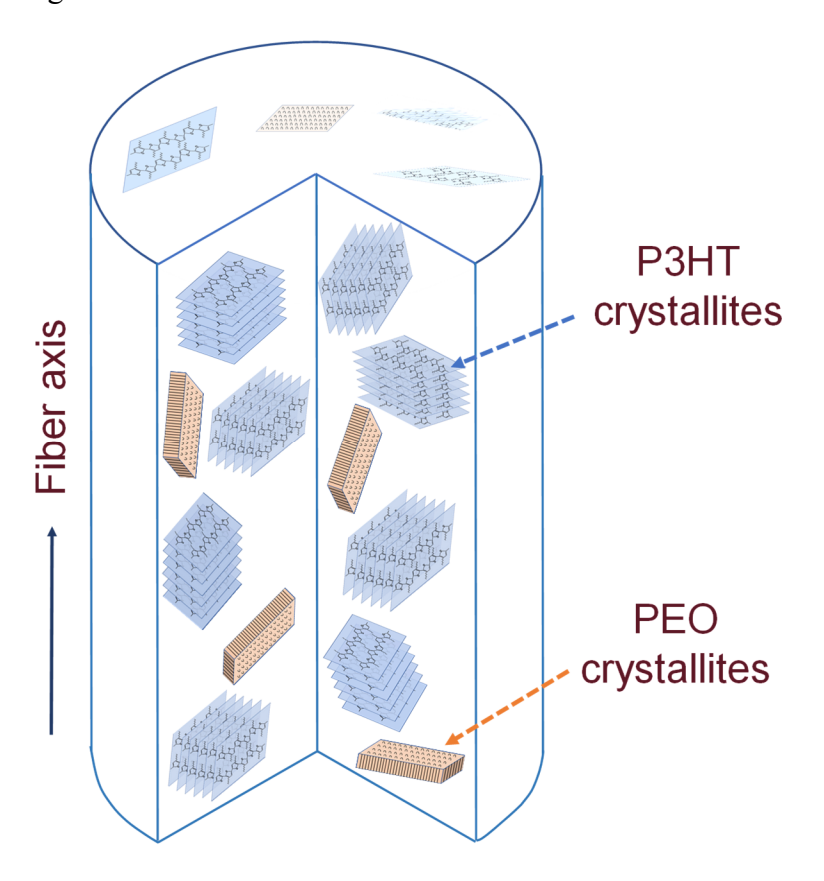
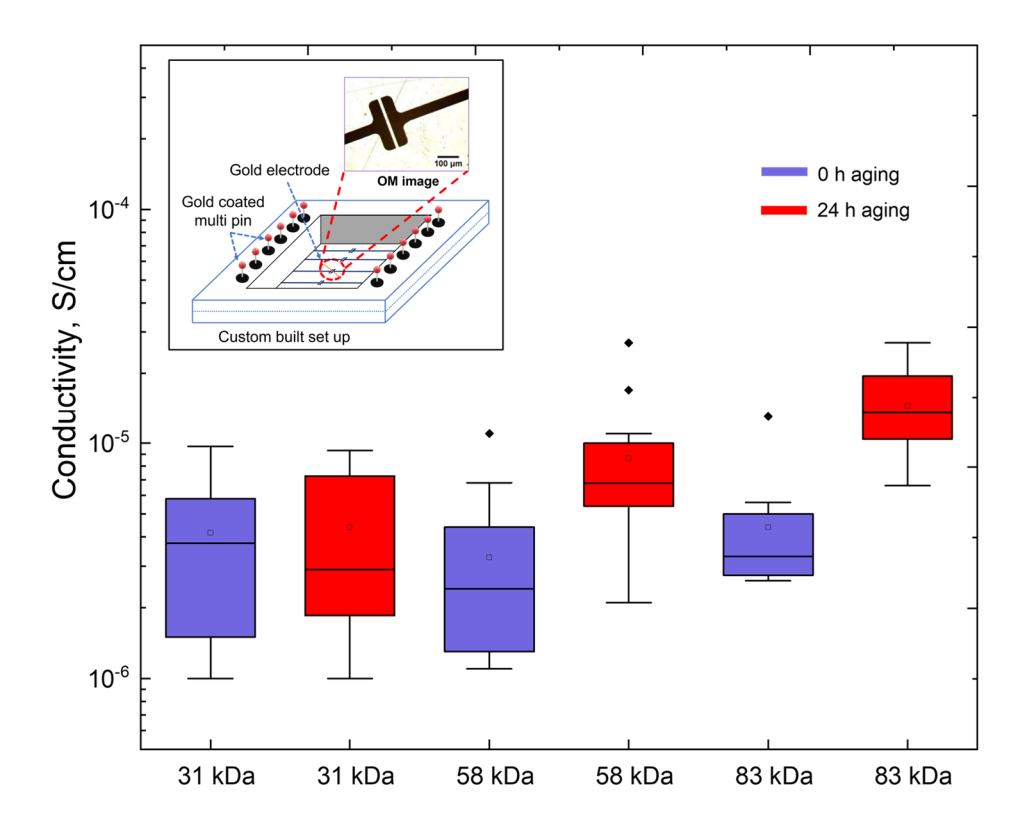


Figure 9. Schematic of a microstructure of fiber (the figure is not drawn to scale).

# **Electrical Conductivity of the Fibers**

We studied the room temperature electrical conductivity of the single electrospun fiber using a custom-built setup and for fiber mats using IDE chips. The fiber mat conductivity values were found to be  $\sim 10^{-7}$  S/cm, two orders of magnitude higher than that reported in the literature. Note that the IDE chips provide the bulk conductivity values which is appropriate for thin films but not for the discontinuous and poorly aligned electrospun fibers as found in fiber mats (see Figure S19). Although most commonly reported in the literature, the bulk conductivity values are not highly beneficial. Instead, the single fiber conductivity values can be directly related to the polymer properties and processing conditions. Here, we aimed to measure the conductivity of

single fiber using a specially designed chip shown in Figure S3a. We targeted to collect a single fiber connecting the two gold contacts on a chip, but because of the experimental challenges, we often collected multiple fibers, as high as four fibers (Figure S3d).



**Figure 10.** Electrical conductivity of P3HT/PEO single fibers as a function of the P3HT molecular weight and aging conditions of the spinning solution. For each condition minimum of 12 sets of samples were characterized.

For our system, the linear current-voltage (I–V) curves confirmed the ohmic behavior of these samples.<sup>23,65</sup> For a single fiber connecting the gold contacts, electrical conductivity ( $\sigma$ ) was obtained by using the following equation (1),

Single fiber conductivity, 
$$\sigma = \frac{1}{\rho} = \frac{l}{V} * \frac{L}{A} = \frac{\frac{l}{V}}{\pi(\frac{R^2}{L})}$$
 (1)

Where A, I, V, L, and R are the fiber cross-sectional area, current, voltage, length, and radius of fiber, respectively. As discussed above, all fibers were considered cylindrical (Figure S8). However, if we have more than one fiber connecting the gold contacts, the equation (1) can be modified as below to estimate the single fiber conductivity,

$$\sigma = \frac{1}{\rho} = \frac{\frac{1}{V}}{\pi \sum_{i=1}^{n} \frac{R_i^2}{L_i}}$$
 (2)

Where  $L_i$  and  $R_i$  are the length and radius of the  $i^{th}$  fiber captured from optical micrographs. I and V are the overall current and applied voltage.

Figure 10 shows the  $\sigma$  for all three molecular weights of P3HT and at the two aging conditions. The molecular weight of P3HT plays a role in  $\sigma$ , particularly for the higher molecular weight, as  $\sigma$  for 83 kDa fibers has been found to be statistically higher than 58 kDa. The aging of the spinning solution played a role on  $\sigma$  for 58 and 83 kDa fibers, but not for 31 kDa fibers.  $\sigma$  increased by two times from 58 kDa\_0h to 58 kDa\_24h fiber. For 83 kDa, the change was more significant. The maximum conductivity of  $2.75 \times 10^{-5}$  S/cm was obtained for the 83 kDa\_24h fibers, which was about five times higher than 83 kDa\_0h. The highly ordered structure in 83 kDa\_24h can be attributed to high conductivity values. Also, the long polymer chains in the high molecular weight of P3HT may work as a tie chain between the ordered region facilitating charge transport. For comparison,  $\sigma$  of blade-coated thin films of pristine 83 kDa P3HT from w/o and w/24h aged solutions are reported in Table S3. The electrical conductivities of the fibers were found to be similar to the pristine 83 kDa P3HT thin films measured here (Table S3) and that reported in the literature. Note that the electrospun fibers considered here contained 25% PEO, an insulating material. In addition to PEO, other flexible polymers will be considered in future research, and

other types of conjugated polymers will also be considered. A future study will also investigate whether the presence of PEO chains has any effect on P3HT self-assembly with aging.

#### **CONCLUSIONS**

In this study, we have successfully processed P3HT/PEO into fibers using the electrospinning technique. We have captured the self-assembly behavior of P3HT in the spinning solution in the presence of PEO. The P3HT/PEO solutions displayed color change during the 24 h aging process, indicating time-dependent polymer aggregation. Correspondingly, the PL data demonstrated that the significant self-assembly/aggregation of P3HT chains occurred for 83 kDa P3HT, the highest molecular weight considered here. The PL data also captured the transformation from J- to Haggregates in solution facilitated by the high molecular weight P3HT and 24 h aging, indicating the interchain exciton coupling by promoting  $\pi$ - $\pi$  stacking of P3HT chains. The preexisting Haggregates in the solution were retained and even increased during the processing of electrospun fibers. The shear-rheometry indicates that the self-assembly of the high molecular weight P3HT chains within the solution led to gelation. We hypothesized that the shear stress in the needle during processing dissociated the gel structure and facilitated the spinning. The GIWAXS analysis for the samples investigated here suggested that polymer crystals were randomly oriented with respect to the fiber axis. This study captured the effect of P3HT molecular weight, PEO concentration, and the aging of the spinning solution on the electrical conductivities. The electrical conductivity of fibers increased with the molecular weight and aging of the solution. As high as five-fold enhancement in single fiber electrical conductivity was obtain-ned for the aged high molecular weight P3HT solution compared to the fibers from the without aged solution.

#### ASSOCIATED CONTENT

Supporting Information. A table presenting the properties of P3HT grades; crystallographic information of P3HT/PEO fiber mats; comparison of thin-film and single fiber conductivity; an image of the experimental setup for P3HT aging in the needle; schematic of rheology setup; gold patterned custom-built setup for single fiber conductivity measurement; temperature profile of spinning solution; SEM micrograph of beads from 12 wt/v% P3HT; OM images of PEO electrospun fibers; progressive transformation of beads to fibers; SEM images of cylindrical fiber; SEM image of sub-micron fibers; color change of P3HT/PEO in chloroform at room temperature due to aging; PL spectra of thin films; steady shear viscosity as a function of shear rate; DSC thermograms of pristine P3HT, PEO powders and fiber mats; DSC of fiber mat including second heating and cooling cycle; XRD raw data; XRD of PEO drop-casted and electrospun fiber mat; IDE chips with fiber mat and thin-film; single fiber and fiber conductivity measurement details.

# **AUTHOR INFORMATION**

# **Corresponding Author**

Santanu Kundu, santanukundu@che.msstate.edu

#### **Author Contributions**

HA and SK designed the experiments and conducted the data analysis and interpretation. HA conducted the experiments. SK conceptualized and oversaw the research. The manuscript was written by HA and SK and included feedback from all authors. SZ and XG performed the GIWAXS experiments and analyzed the data; MG assisted in designing a custom-built device holder for single fiber conductivity measurements; CL and JA provided the Au patterned electrode

chips and carried out the initial single fiber conductivity measurements. All authors have approved the final version of the manuscript.

# **Funding sources**

This material is based on work supported by the National Science Foundation under Grant No. 1757220.

# Notes

The authors declare no competing financial interest.

# ACKNOWLEDGMENT

The authors acknowledge Dr. Lifeng Huang for assisting in the preliminary single fiber conductivity measurement.

#### REFERENCES

- (1) Kuo, C. C.; Wang, C. T.; Chen, W. C. Poly(3-Hexylthiophene)/Poly(Methyl Methacrylate) Core-Shell Electrospun Fibers for Sensory Applications. *Macromol. Symp.* 2009, *279* (1), 41–47. https://doi.org/10.1002/masy.200950506.
- (2) Nanofibers, P.; Lee, S. W.; Lee, H. J.; Choi, J. H.; Koh, W. G.; Myoung, J. M.; Hur, J. H.; Park, J. J.; Cho, J. H.; Jeong, U. Periodic Array of Polyelectrolyte-Gated Organic Transistors from Electrospun. 2010, 347–351. https://doi.org/10.1021/nl903722z.
- (3) Sundarrajan, S.; Murugan, R.; Nair, A. S.; Ramakrishna, S. Fabrication of P3HT/PCBM Solar Cloth by Electrospinning Technique. *Mater. Lett.* 2010, *64* (21), 2369–2372. https://doi.org/10.1016/j.matlet.2010.07.054.
- (4) Chen, J. Y.; Wu, H. C.; Chiu, Y. C.; Lin, C. J.; Tung, S. H.; Chen, W. C. Electrospun Poly(3-Hexylthiophene) Nanofibers with Highly Extended and Oriented Chains through Secondary Electric Field for High-Performance Field-Effect Transistors. *Adv. Electron. Mater.* 2015, *I* (1–2), 3–6. https://doi.org/10.1002/aelm.201400028.
- (5) Chen, J. Y.; Kuo, C. C.; Lai, C. S.; Chen, W. C.; Chen, H. L. Manipulation on the Morphology and Electrical Properties of Aligned Electrospun Nanofibers of Poly(3-Hexylthiophene) for Field-Effect Transistor Applications. *Macromolecules* 2011, 44 (8), 2883–2892. https://doi.org/10.1021/ma102286m.
- (6) Kleinhenz, N.; Rosu, C.; Chatterjee, S.; Chang, M.; Nayani, K.; Xue, Z.; Kim, E.; Middlebrooks, J.; Russo, P. S.; Park, J. O.; Srinivasarao, M.; Reichmanis, E. Liquid Crystalline

- Poly(3-Hexylthiophene) Solutions Revisited: Role of Time-Dependent Self-Assembly. *Chem. Mater.* 2015, *27* (7), 2687–2694. https://doi.org/10.1021/acs.chemmater.5b00635.
- (7) Persson, N. E.; Chu, P. H.; McBride, M.; Grover, M.; Reichmanis, E. Nucleation, Growth, and Alignment of Poly(3-Hexylthiophene) Nanofibers for High-Performance OFETs. *Acc. Chem. Res.* 2017, *50* (4), 932–942. https://doi.org/10.1021/acs.accounts.6b00639.
- (8) Park, B.; Aiyar, A.; Park, M. S.; Srinivasarao, M.; Reichmanis, E. Conducting Channel Formation in Poly(3-Hexylthiophene) Field Effect Transistors: Bulk to Interface. *J. Phys. Chem. C* 2011, *115* (23), 11719–11726. https://doi.org/10.1021/jp111677x.
- (9) Aiyar, A. R.; Hong, J. II; Reichmanis, E. Regioregularity and Intrachain Ordering: Impact on the Nanostructure and Charge Transport in Two-Dimensional Assemblies of Poly(3-Hexylthiophene). *Chem. Mater.* 2012, *24* (15), 2845–2853. https://doi.org/10.1021/cm202700k.
- (10) Liu, J.; Mikhaylov, I. A.; Zou, J.; Osaka, I.; Masunov, A. E.; McCullough, R. D.; Zhai, L. Insight into How Molecular Structures of Thiophene-Based Conjugated Polymers Affect Crystallization Behaviors. *Polymer (Guildf)*. 2011, *52* (10), 2302–2309. https://doi.org/10.1016/j.polymer.2011.03.026.
- (11) Zhai, L.; Khondaker, S. I.; Thomas, J.; Shen, C.; Mcinnis, M. Ordered Conjugated Polymer Nano- and Microstructures: Structure Control For. *Nano Today* 2015, *9* (6), 705–721. https://doi.org/10.1016/j.nantod.2014.10.004.
- (12) Giri, G.; Delongchamp, D. M.; Reinspach, J.; Fischer, D. A.; Richter, L. J.; Xu, J.; Benight, S.; Ayzner, A.; He, M.; Fang, L.; Xue, G.; Toney, M. F.; Bao, Z. Effect of Solution Shearing

Method on Packing and Disorder of Organic Semiconductor Polymers. *Chem. Mater.* 2015, 27 (7), 2350–2359. https://doi.org/10.1021/cm503780u.

- (13) Koch, F. P. V.; Rivnay, J.; Foster, S.; Müller, C.; Downing, J. M.; Buchaca-Domingo, E.; Westacott, P.; Yu, L.; Yuan, M.; Baklar, M.; Fei, Z.; Luscombe, C.; McLachlan, M. A.; Heeney, M.; Rumbles, G.; Silva, C.; Salleo, A.; Nelson, J.; Smith, P.; Stingelin, N. The Impact of Molecular Weight on Microstructure and Charge Transport in Semicrystalline Polymer Semiconductors-Poly(3-Hexylthiophene), a Model Study. *Prog. Polym. Sci.* 2013, *38* (12), 1978–1989. https://doi.org/10.1016/j.progpolymsci.2013.07.009.
- (14) Brinkmann, M.; Rannou, P. Molecular Weight Dependence of Chain Packing and Semicrystalline Structure in Oriented Films of Regioregular Poly(3-Hexylthiophene)Revealed by High-Resolution Transmission Electron Microscopy. *Macromolecules* 2009, *42* (4), 1125–1130. https://doi.org/10.1021/ma8023415.
- (15) Mauer, B. R.; Kastler, M. The Impact of Polymer Regioregularity on Charge Transport and Efficiency of P3HT: PCBM Photovoltaic Devices. https://doi.org/10.1002/adfm.201000320.
- (16) Chang, M.; Lim, G. T.; Park, B.; Reichmanis, E. Control of Molecular Ordering, Alignment, and Charge Transport in Solution-Processed Conjugated Polymer Thin Films. *Polymers (Basel)*. 2017, *9* (6), 23–31. https://doi.org/10.3390/polym9060212.
- (17) Park, M. S.; Aiyar, A.; Park, J. O.; Reichmanis, E.; Srinivasarao, M. Solvent Evaporation Induced Liquid Crystalline Phase in Poly(3-Hexylthiophene). *J. Am. Chem. Soc.* 2011, *133* (19), 7244–7247. https://doi.org/10.1021/ja110060m.

- (18) Chen, J. Y.; Hsieh, H. C.; Chiu, Y. C.; Lee, W. Y.; Hung, C. C.; Chueh, C. C.; Chen, W. C. Electrospinning-Induced Elastomeric Properties of Conjugated Polymers for Extremely Stretchable Nanofibers and Rubbery Optoelectronics. *J. Mater. Chem. C* 2020, 8 (3), 873–882. https://doi.org/10.1039/c9tc05075b.
- (19) Serrano-Garcia, W.; Bonadies, I.; Thomas, S.; Guarino, V. P3HT Loaded Piezoelectric Electrospun Fibers for Tunable Molecular Adsorption. *Mater. Lett.* 2020, *266*, 127458. https://doi.org/10.1016/j.matlet.2020.127458.
- (20) Pierini, F.; Lanzi, M.; Nakielski, P.; Pawłowska, S.; Zembrzycki, K.; Kowalewski, T. A. Electrospun Poly(3-Hexylthiophene)/Poly(Ethylene Oxide)/Graphene Oxide Composite Nanofibers: Effects of Graphene Oxide Reduction. *Polym. Adv. Technol.* 2016, *27* (11), 1465–1475. https://doi.org/10.1002/pat.3816.
- (21) Chen, J. Y.; Wu, H. C.; Chiu, Y. C.; Lin, C. J.; Tung, S. H.; Chen, W. C. Electrospun Poly(3-Hexylthiophene) Nanofibers with Highly Extended and Oriented Chains through Secondary Electric Field for High-Performance Field-Effect Transistors. *Adv. Electron. Mater.* 2015, *I* (1–2), 1–8. https://doi.org/10.1002/aelm.201400028.
- (22) Bianco, A.; Bertarelli, C.; Frisk, S.; Rabolt, J. F.; Gallazzi, M. C.; Zerbi, G. Electrospun Polyalkylthiophene/Polyethyleneoxide Fibers: Optical Characterization. *Synth. Met.* 2007, *157* (6–7), 276–281. https://doi.org/10.1016/j.synthmet.2007.03.006.
- (23) Chan, K. H. K.; Yamao, T.; Kotaki, M.; Hotta, S. Unique Structural Features and Electrical Properties of Electrospun Conjugated Polymer Poly(3-Hexylthiophene) (P3HT) Fibers. *Synth. Met.* 2010, *160* (23–24), 2587–2595. https://doi.org/10.1016/j.synthmet.2010.10.009.

- (24) Laforgue, A.; Robitaille, L. Fabrication of Poly-3-Hexylthiophene/Polyethylene Oxide Nanofibers Using Electrospinning. *Synth. Met.* 2008, *158* (14), 577–584. https://doi.org/10.1016/j.synthmet.2008.04.004.
- (25) Hernández-Martínez, D.; Martínez-Alonso, C.; Castillo-Ortega, M. M.; Arenas-Arrocena, M. C.; Nicho, M. E. Preparation and Characterization of Electrospun Fibers Containing Poly(3-Hexylthiophene) and Poly(3-Hexylthiophene)/CdS. *Synth. Met.* 2015, 209, 496–501. https://doi.org/10.1016/j.synthmet.2015.09.001.
- (26) Hernández-Martínez, D.; Nicho, M. E.; Hu, H.; León-Silva, U.; Arenas-Arrocena, M. C.; García-Escobar, C. H. Electrospinning of P3HT-PEO-CdS Fibers by Solution Method and Their Properties. *Mater. Sci. Semicond. Process.* 2017, *61* (November 2016), 50–56. https://doi.org/10.1016/j.mssp.2016.12.039.
- (27) González, R.; Pinto, N. J. Electrospun Poly(3-Hexylthiophene-2,5-Diyl) Fiber Field Effect Transistor. *Synth. Met.* 2005, *151* (3), 275–278. https://doi.org/10.1016/j.synthmet.2005.05.007.
- (28) Lee, S.; Moon, G. D.; Jeong, U. Continuous Production of Uniform Poly(3-Hexylthiophene) (P3HT) Nanofibers by Electrospinning and Their Electrical Properties. *J. Mater. Chem.* 2009, *19* (6), 743–748. https://doi.org/10.1039/b814833c.
- (29) Liu, H.; Reccius, C. H.; Craighead, H. G. Single Electrospun Regioregular Poly(3-Hexylthiophene) Nanofiber Field-Effect Transistor. *Appl. Phys. Lett.* 2005, 87 (25), 1–3. https://doi.org/10.1063/1.2149980.
- (30) Wu, Q.; Mei, C.; Zhang, X.; Lei, T.; Zhang, Z.; Li, M. Electrospun Poly(Ethylene Oxide) Fibers Reinforced with Poly (Vinylpyrrolidone) Polymer and Cellulose Nanocrystals.

- Electrospinning Method Used to Creat. Funct. Nanocomposites Film. 2018. https://doi.org/10.5772/intechopen.76392.
- (31) Himmelberger, S.; Vandewal, K.; Fei, Z.; Heeney, M.; Salleo, A. Role of Molecular Weight Distribution on Charge Transport in Semiconducting Polymers. *Macromolecules* 2014, *47* (20), 7151–7157. https://doi.org/10.1021/ma501508j.
- (32) Kline, R. J.; McGehee, M. D.; Kadnikova, E. N.; Liu, J.; Fréchet, J. M. J.; Toney, M. F. Dependence of Regioregular Poly(3-Hexylthiophene) Film Morphology and Field-Effect Mobility on Molecular Weight. *Macromolecules* 2005, 38 (8), 3312–3319. https://doi.org/10.1021/ma047415f.
- (33) Bielecka, U.; Lutsyk, P.; Janus, K.; Sworakowski, J.; Bartkowiak, W. Effect of Solution Aging on Morphology and Electrical Characteristics of Regioregular P3HT FETs Fabricated by Spin Coating and Spray Coating. *Org. Electron.* 2011, *12* (11), 1768–1776. https://doi.org/10.1016/j.orgel.2011.06.027.
- (34) Kim, D. K.; Hwang, M.; Lagerwall, J. P. F. Liquid Crystal Functionalization of Electrospun Polymer Fibers. *J. Polym. Sci. Part B Polym. Phys.* 2013, *51* (11), 855–867. https://doi.org/10.1002/polb.23285.
- (35) Aiyar, A. R.; Hong, J. Il; Izumi, J.; Choi, D.; Kleinhenz, N.; Reichmanis, E. Ultrasound-Induced Ordering in Poly(3-Hexylthiophene): Role of Molecular and Process Parameters on Morphology and Charge Transport. *ACS Appl. Mater. Interfaces* 2013, *5* (7), 2368–2377. https://doi.org/10.1021/am3027822.

- (36) Wang, G.; Persson, N.; Chu, P. H.; Kleinhenz, N.; Fu, B.; Chang, M.; Deb, N.; Mao, Y.; Wang, H.; Grover, M. A.; Reichmanis, E. Microfluidic Crystal Engineering of π-Conjugated Polymers. *ACS Nano* 2015, *9* (8), 8220–8230. https://doi.org/10.1021/acsnano.5b02582.
- (37) Niles, E. T.; Roehling, J. D.; Yamagata, H.; Wise, A. J.; Spano, F. C.; Moule, A. J.; Grey, J. K. J-Aggregate Behavior in Poly-3-Hexylthiophene Nanofibers. *Phys. Chem.Lett.* 2012, 3, 2, 259–263. https://doi.org/10.1021/jz201509h.
- (38) Lakdusinghe, M.; Abbaszadeh, M.; Mishra, S.; Sengottuvelu, D.; Wijayapala, R.; Zhang, S.; Benasco, A. R.; Gu, X.; Morgan, S. E.; Wipf, D. O.; Kundu, S. Nanoscale Self-Assembly of Poly(3-Hexylthiophene) Assisted by a Low-Molecular-Weight Gelator toward Large-Scale Fabrication of Electrically Conductive Networks. 2021. https://doi.org/10.1021/acsanm.1c01294.
- (39) Shenoy, S. L.; Bates, W. D.; Frisch, H. L.; Wnek, G. E. Role of Chain Entanglements on Fiber Formation during Electrospinning of Polymer Solutions: Good Solvent, Non-Specific Polymer-Polymer Interaction Limit. *Polymer (Guildf)*. 2005, 46 (10), 3372–3384. https://doi.org/10.1016/j.polymer.2005.03.011.
- (40) Chronakis, I. S.; Grapenson, S.; Jakob, A. Conductive Polypyrrole Nanofibers via Electrospinning: Electrical and Morphological Properties. *Polymer (Guildf)*. 2006, 47 (5), 1597–1603. https://doi.org/10.1016/j.polymer.2006.01.032.
- (41) Yeong, B.; Park, D.; Lee, H. S.; Choi, Y. J.; Kwak, D.; Cho, H.; Lee, S.; Cho, K. Solubility-Induced Ordered Polythiophene Precursors for High-Performance Organic Thin-Film Transistors. https://doi.org/10.1002/adfm.200801763.

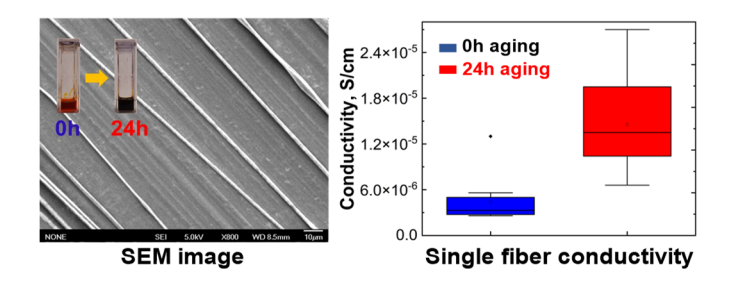
- (42) Wolf, C. M.; Guio, L.; Scheiwiller, S. C.; Hara, R. P. O.; Luscombe, C. K.; Pozzo, L. D. Blend Morphology in Polythiophene Polystyrene Composites from Neutron and X Ray Scattering. 2021. https://doi.org/10.1021/acs.macromol.0c02512.
- (43) Chen, C.; Chan, S.; Li, J.; Wu, K.; Chen, H.; Chen, J.; Huang, W.; Chen, S. Formation and Thermally-Induced Disruption of Nanowhiskers in Poly (3-Hexylthiophene)/ Xylene Gel Studied by Small-Angle X-Ray Scattering. 2010, 7305–7311. https://doi.org/10.1021/ma1008034.
- (44) Kajiya, D.; Saitow, K. I. Ultrapure Films of Polythiophene Derivatives Are Born on a Substrate by Liquid Flow. *ACS Appl. Energy Mater.* 2018, *1* (12), 6881–6889. https://doi.org/10.1021/acsaem.8b01260.
- (45) Spano, F. C.; Silva, C. H- and J-Aggregate Behavior in Polymeric Semiconductors. *Annu. Rev. Phys. Chem.* 2014, 65 (January), 477–500. https://doi.org/10.1146/annurev-physchem-040513-103639.
- (46) Spano, F. C. The Spectral Signatures of Frenkel Polarons in H- And J-Aggregates. *Acc. Chem. Res.* 2010, 43 (3), 429–439. https://doi.org/10.1021/ar900233v.
- (47) Martin, T. P.; Wise, A. J.; Busby, E.; Gao, J.; Roehling, J. D.; Ford, M. J.; Larsen, D. S.; Moulé, A. J.; Grey, J. K. Packing Dependent Electronic Coupling in Single Poly(3-Hexylthiophene) H- and J-Aggregate Nanofibers. *J. Phys. Chem. B* 2013, *117* (16), 4478–4487. https://doi.org/10.1021/jp308586k.
- (48) Kim, T.; Im, J. H.; Choi, H. S.; Yang, S. J.; Kim, S. W.; Park, C. R. Preparation and Photoluminescence (PL) Performance of a Nanoweb of P3HT Nanofibers with Diameters below 100 Nm. *J. Mater. Chem.* 2011, *21* (37), 14231–14239. https://doi.org/10.1039/c1jm10396b.

- (49) Hashemnejad, S. M.; Kundu, S. Rheological Properties and Failure of Alginate Hydrogels with Ionic and Covalent Crosslinks. *Soft Matter* 2019, *15* (39), 7852–7862. https://doi.org/10.1039/c9sm01039d.
- (50) Mishra, S.; Badani Prado, R. M.; Kundu, S. Concentration-Dependent Mechanical Behavior of Physically Assembled Triblock Copolymer Gels. *ACS Appl. Polym. Mater.* 2020, *2* (12), 5388–5397. https://doi.org/10.1021/acsapm.0c00583.
- (51) Prado, R. M. B.; Mishra, S.; Ahmad, H.; Burghardt, W. R.; Kundu, S. Capturing the Transient Microstructure of a Physically Assembled Gel Subjected to Temperature and Large Deformation. *Macromolecules* 2021, 54 (19), 8946–8959. https://doi.org/10.1021/acs.macromol.1c00895.
- (52) Hashemnejad, S. M.; Kundu, S. Probing Gelation and Rheological Behavior of a Self-Assembled Molecular Gel. *Langmuir* 2017, *33* (31), 7769–7779. https://doi.org/10.1021/acs.langmuir.7b01531.
- (53) Newbloom, G. M.; Iglesia, P. De; Pozzo, L. D. Bulk and in Thin- Fi Lms Using Low Volatility Solvent /. 2014, 8945–8954. https://doi.org/10.1039/c4sm00960f.
- (54) Newbloom, G. M.; Weigandt, K. M.; Pozzo, D. C. Electrical, Mechanical, and Structural Characterization of Self-Assembly in Poly(3-Hexylthiophene) Organogel Networks. *Macromolecules* 2012, *45* (8), 3452–3462. https://doi.org/10.1021/ma202564k.
- (55) Newbloom, G. M.; Kim, F. S.; Jenekhe, S. A.; Pozzo, D. C. Mesoscale Morphology and Charge Transport in Colloidal Networks of Poly(3-Hexylthiophene). *Macromolecules* 2011, *44* (10), 3801–3809. https://doi.org/10.1021/ma2000515.

- (56) Samitsu, S.; Shimomura, T.; Ito, K. Nanofiber Preparation by Whisker Method Using Solvent-Soluble Conducting Polymers. 2008, 516, 2478–2486. https://doi.org/10.1016/j.tsf.2007.04.058.
- (57) Merchiers, J.; Martínez Narváez, C. D. V.; Slykas, C.; Reddy, N. K.; Sharma, V. Evaporation and Rheology Chart the Processability Map for Centrifugal Force Spinning. *Macromolecules* 2021, *54* (23), 11061–11073. https://doi.org/10.1021/acs.macromol.1c01799.
- (58) Xu, X.; Jiang, L.; Zhou, Z.; Wu, X.; Wang, Y. Preparation and Properties of Electrospun Soy Protein Isolate/Polyethylene Oxide Nanofiber Membranes. *ACS Appl. Mater. Interfaces* 2012, 4 (8), 4331–4337. https://doi.org/10.1021/am300991e.
- (59) Zembrzycki, K.; Kowalewski, T. A. Single-Material Organic Solar Cells Based on Electrospun Fullerene- Grafted Polythiophene Nano Fi Bers. 2017. https://doi.org/10.1021/acs.macromol.7b00857.
- (60) Snyder, C. R.; Nieuwendaal, R. C.; Delongchamp, D. M.; Luscombe, C. K.; Sista, P.; Boyd,
  S. D. Quantifying Crystallinity in High Molar Mass Poly(3-Hexylthiophene). *Macromolecules*2014, 47 (12), 3942–3950. https://doi.org/10.1021/ma500136d.
- (61) Shen, X.; Hu, W.; Russell, T. P. Measuring the Degree of Crystallinity in Semicrystalline Regioregular Poly(3-Hexylthiophene). 2016, 4–12. https://doi.org/10.1021/acs.macromol.6b00799.
- (62) Na, J. Y.; Kang, B.; Park, Y. D. In Fl Uence of Molecular Weight on the Solidi Fi Cation of a Semiconducting Polymer during Time-Controlled Spin-Coating. 2019. https://doi.org/10.1021/acs.jpcc.9b03203.

- (63) Deitzel, J. M.; Kleinmeyer, J.; Harris, D.; Beck Tan, N. C. The Effect of Processing Variables on the Morphology of Electrospun. *Polymer (Guildf)*. 2001, 42, 261–272. https://doi.org/10.1016/S0032-3861(00)00250-0.
- (64) Arlauskas, K.; Viliu, M.; Genevic, K.; Jus, G.; Stubb, H. Charge Transport in π-Conjugated Polymers. *Phys. Rev. B* 2000, *62* (24), 235–238. https://doi.org/10.1103/PhysRevB.62.R16235.
- (65) Lee, J. Y.; Kang, T. H.; Choi, J. H.; Choi, I. S.; Yu, W. R. Improved Electrical Conductivity of Poly(Ethylene Oxide) Nanofibers Using Multi-Walled Carbon Nanotubes. *AIP Adv.* 2018, *8* (3). https://doi.org/10.1063/1.5026509.
- (66) Jacobs, I. E.; Aasen, E. W.; Oliveira, J. L.; Fonseca, T. N.; Roehling, J. D.; Li, J.; Zhang, G.; Augustine, M. P.; Mascal, M.; Moulé, A. J. Comparison of Solution-Mixed and Sequentially Processed P3HT:F4TCNQ Films: Effect of Doping-Induced Aggregation on Film Morphology. *J. Mater. Chem. C* 2016, *4* (16), 3454–3466. https://doi.org/10.1039/c5tc04207k.
- (67) Lim, E.; Peterson, K. A.; Su, G. M.; Chabinyc, M. L. Thermoelectric Properties of Poly(3-Hexylthiophene) (P3HT) Doped with 2,3,5,6-Tetrafluoro-7,7,8,8-Tetracyanoquinodimethane (F4TCNQ) by Vapor-Phase Infiltration. *Chem. Mater.* 2018, *30* (3), 998–1010. https://doi.org/10.1021/acs.chemmater.7b04849.

# For Table of Contents use only



# Effects of Poly(3-hexylthiophene) Molecular Weight and the Aging of Spinning Solution on the Electrospun Fiber Properties

Humayun Ahmad,  $^{\dagger}$  Song Zhang,  $^{\ddagger}$  Chih-Ting Liu,  $^{\ddagger}$  Jason D. Azoulay,  $^{\ddagger}$  Xiaodan Gu,  $^{\ddagger}$  Mahesh K Gangishetty,  $^{\dagger}$  Santanu Kundu $^{\dagger}*$ 

<sup>†</sup>Dave C. Swalm School of Chemical Engineering, Mississippi State University, MS State, MS 39762, United States

<sup>‡</sup> School of Polymer Science and Engineering, University of Southern Mississippi, Hattiesburg,

MS 39406, USA

Department of Chemistry & Department of Physics and Astronomy, Mississippi State
University, MS State, MS 39762, United States